INORGANIC CHEMISTRY
FRONTIERS

RESEARCH ARTICLE

View Article Online
View Journal | View Issue

Cite this: *Inorg. Chem. Front.*, 2024, **11**, 6387

Construction of an oxygen vacancy-enriched triple perovskite oxide electrocatalyst for efficient and stable oxygen evolution in acidic media†

Yuanyuan Wu,[a] Tixuan Xia,[b] Lu Yang,[a] Feifan Guo,[c] Wei Jiang,[b] Jihui Lang,[d] Yunchao Ma,[a] Jingdong Feng,[a] Guangbo Che *[e] and Chunbo Liu[b]

The development of anodic electrocatalysts toward the oxygen evolution reaction (OER) in harsh acidic environments faces significant challenges of low efficiency, instability and high cost. Ru-based oxides exhibit remarkable initial activity toward the OER, but the presence of soluble high-valence oxygen-vacancy intermediates can accelerate the dissolution of Ru species. In this study, a triple $Sr_2CaRu_2IrO_9$ perovskite oxide electrocatalyst has been successfully synthesized, demonstrating a low overpotential of 172 mV at 10 mA cm^{-2} and excellent stability for over 75 hours. The introduction of dual-site heteroatoms leads to the generation of oxygen vacancies, which control the excessive lattice oxygen participating in the OER *via* the lattice oxygen oxidation mechanism (LOM). This effectively prevents the excessive oxidation of Ru to form soluble $Ru^{>4+}$ species. Density functional theory (DFT) calculations show that the negative shift of O 2p and Ru 4d band centers weakens the covalency of Ru–O, optimizes the adsorption energy of oxygen intermediates, and thus improves the inherent catalytic activity and stability.

Received 18th June 2024,
Accepted 13th August 2024

DOI: 10.1039/d4qi01536c

rsc.li/frontiers-inorganic

Introduction

Hydrogen is widely recognized as an ideal energy carrier, boasting numerous advantages such as its diverse sources, high caloric value, clean and carbon-free properties, and versatile applications. It plays a pivotal role in promoting the clean and efficient utilization of traditional fossil energy sources and supporting the large-scale development of renewable energy.[1–3] In the commercial sector, proton exchange membrane water electrolyzer (PEMWE) and alkaline water electrolyzer (AWE) technologies are the two primary methods for hydrogen production. Among these methods, PEMWE stands out for its exceptional efficiency due to its high proton conductivity, low impedance, rapid dynamic response, high hydrogen pressure, and high purity.[4–9] However, the widespread adoption of PEMWE faces challenges due to the sluggish kinetics of the anodic oxygen evolution reaction (OER) and the limited stability of acidic electrocatalysts. Consequently, developing efficient and stable acidic OER catalysts is paramount for advancing PEMWE hydrogen production technologies.[10–12] Significant research efforts are focused on designing and developing innovative catalysts that exhibit enhanced catalytic activity and long-term stability. These catalysts aim to improve the kinetics of the OER while minimizing degradation under harsh acidic conditions.

Among the various catalysts, only noble metals such as Ir- and Ru-based catalysts have demonstrated the ability to maintain good catalytic performance under strongly acidic and strong oxidation conditions.[13–18] However, the high cost, rarity and lack of corrosion resistance under strongly acidic conditions of Ir- and Ru-based catalysts have prevented their widespread application in PEMWEs. Perovskite oxides (ABO_3) containing low loading precious metals are a kind of promising acidic OER catalysts.[19–24] In the perovskite structure, the A-site and B-site elements can be partially or completely replaced by other metal ions. This offers a vast array of physical and

[a]*Key Laboratory of Preparation Application of Environmental Friendly Materials, Ministry of Education, College of Chemistry, Jilin Normal University, Siping 136000, P. R. China*
[b]*Jilin Joint Technology Innovation Laboratory of Developing and Utilizing Materials of Reducing Pollution and Carbon Emissions, College of Engineering, Jilin Normal University, Siping, 136000, P. R. China. E-mail: chunboliu@jlnu.edu.cn*
[c]*Key Laboratory of Polyoxometalate and Reticular Material Chemistry of Ministry of Education, Faculty of Chemistry, Northeast Normal University, Changchun, 130024, China*
[d]*Key Laboratory of Functional Materials Physics and Chemistry of the Ministry of Education, Jilin Normal University, Changchun, 130103, China*
[e]*College of Chemistry, Baicheng Normal University, Baicheng, 13700, P. R. China. E-mail: guangboche@jnu.edu.cn*

†Electronic supplementary information (ESI) available. See DOI: https://doi.org/10.1039/d4qi01536c

chemical features, allowing for the construction of a wide range of high-performing water oxidation catalysts with limitless development potential. In addition, the coupling of Ir and Ru metals is also an effective strategy to solve the above limitations and improve catalyst performance. For example, Liu *et al.* reported that an iridium-doped ruthenium salt pyrochlore $Y_2Ru_{1.2}Ir_{0.8}O_7$ exhibits excellent OER activity and stability in acidic electrolytes.[25] The synergistic effect of Ir and Ru sites allows the ruthenium and iridium in pyrochlore to maintain a lower oxidation state during the catalytic process, which prevents the overoxidation of ruthenium during the OER and also reduces the formation of OOH* intermediates. Wang *et al.* reported an ultrathin nanocage $Ir_{0.5}Ru_{0.5}O_2$ that can reach 10 mA cm^{-2} with only 215 mV during the acidic OER. This excellent performance is attributed to the effective combination of Ru and Ir.[26] During the catalytic process, $Ir_{0.5}Ru_{0.5}$ tends to oxidize Ir to form $Ir_{0.5}Ru_{0.5}O_2$, which inhibits the formation of soluble $Ru^{>4+}$ and ensures the long-term durability of the material. Yang *et al.* designed a B-site substituted Ruddlesden–Popper phase $Sr_2(Ru_xIr_{1-x})O_4$ acidic catalyst.[27] The results show that the partial substitution of the B site element optimizes the electronic structure and crystal structure of $Sr_2(Ru_xIr_{1-x})O_4$, resulting in a greater number of hydroxyl groups and spatial overlap of Ru 4d/Ir 5d–O orbitals on its surface, which are beneficial in improving the performance of the OER.

In addition, different catalytic mechanisms will also affect the performance of the catalyst. The traditional adsorbed evolution mechanism (AEM) and lattice oxygen oxidation mechanism (LOM) are the two most widely accepted OER mechanisms.[28–32] At present, there is a lot of controversy about the presence of OER effects in the LOM. In fact, the direct O–O coupling of the LOM can bypass the adsorption energy limitation of $\Delta G_{OH^*} - \Delta G_{OOH^*}$ and facilitate the OER reaction kinetics.[33,34] However, this enhanced reaction kinetics will come at the expense of catalyst stability.[35,36] Therefore, it is critical to balance the relationship between catalytic activity and stability of catalysts by regulating the involvement of the AEM and LOM during OER progress.

In this study, a $Sr_2CaRu_2IrO_9$ perovskite oxide catalyst with dual-site regulation has been synthesized for acidic water oxidation. The introduction of heteroatoms leads to the formation of an appropriate amount of oxygen vacancies. This ultimately enhances the catalytic activity of the catalyst. $Sr_2CaRu_2IrO_9$ demonstrates a current density of 10 mA cm^{-2} at an overpotential of only 172 mV in 0.5 M H_2SO_4, and maintains its catalytic performance for more than 75 hours. Its performance surpasses those of $Sr_3Ru_2IrO_9$, $SrRuO_3$, and RuO_2 by a significant margin. DFT calculations demonstrate that the substitution of Ca and Ir induces a negative shift in the centers of O 2p and Ru 4d, leading to a weakening of the adsorption energy of oxygen species intermediates. Simultaneously, the formation of oxygen vacancies weakens the covalency of metal–oxygen bonds, thereby inhibiting excessive lattice oxygen from participating in the OER and improving the stability of the catalyst.

Experimental

Synthesis of $Sr_xCa_{3-x}Ru_2IrO_9$

Taking $Sr_2CaRu_2IrO_9$ as an example, the synthesis method is as follows: mix 68.15 mg calcium carbonate, 140 mg strontium acetate ($C_4H_6O_4Sr$) and 280 mg citric acid ($C_6H_8O_7$) with 5 mL deionized water to form solution A and mix 15.83 mg ruthenium trichloride hydrate ($RuCl_3{\cdot}xH_2O$), 20.04 mg potassium hexachloroiridate(IV) (K_2IrCl_6) and 4 mL ethylene glycol ($(CH_2OH)_2$) to form solution B. Add solution B to solution A dropwise, and mix evenly with a magnetic stirrer to obtain solution C. Transfer solution C to an oven and dry at 150 °C for 12 hours to obtain a brown solid. Transfer the solid precursor obtained to a tube furnace and subject to calcination at sequential gradient temperatures of 300 °C (for 6 hours), 500 °C (for 3 hours), and 700 °C (for 6 hours) with a heating rate of 3 °C min^{-1}. For the synthesis of other ratios of $Sr_xCa_{3-x}Ru_2IrO_9$, the experimental process is almost the same as that of the perovskite with $Sr_2CaRu_2IrO_9$, except that the $CaCO_3$ and $C_4H_6O_4Sr$ are changed.

For the synthesis of other ratios of $Sr_3Ru_2IrO_9$, the experimental process is almost the same as that of $Sr_2CaRu_2IrO_9$, except that calcium carbonate is not added. The synthetic procedure of $SrRuO_3$ was similar to that of $Sr_xCa_{3-x}Ru_2IrO_9$ without the addition of calcium carbonate and potassium hexachloroiridate(IV).

Electrochemical measurements

All electrochemical measurements were performed by using a CHI 760E three-electrode system. A catalyst-coated glassy carbon (GC) electrode with a diameter of 3 mm was used as the working electrode, a platinum wire was used as the counter electrode, and a saturated calomel electrode (SCE) was used as the reference electrode. The working electrode was prepared as follows: 3.5 mg catalyst was ultrasonically dispersed in 50 μL isopropanol solution to prepare a catalyst ink as solution 1. Finally, 5 μL of solution 1 were deposited on a glassy carbon electrode with a diameter of 3 mm and allowed to dry naturally. The linear sweep voltammetry (LSV) measurements were performed at a scan rate of 1 mV s^{-1} without *iR*-drop compensation. Electrochemical impedance spectroscopy (EIS) was performed from 100 kHz to 0.05 Hz with a voltage perturbation of 5 mV. All the DFT calculations were conducted based on the Vienna *ab initio* simulation package (VASP). The values of turnover frequency (TOF) are calculated, assuming that all Ru and Ir ions in the catalysts are active and contribute to the catalytic reaction. The faradaic efficiency is determined through constant current testing in a three-electrode electrolytic cell. The faradaic efficiency is defined as the ratio of experimentally determined O_2 to theoretically expected O_2 from the reaction. We collected the evolved O_2 using water drainage and calculated the moles of O_2 based on gas laws.

Results and discussion

Ru-based perovskite oxides are prone to deactivation as acidic OER catalysts.[33–39] The catalytic performance can be effectively enhanced by regulating the B site, particularly through the coupling of Ir–Ru. Initially, we investigated the impact of B site regulation on the catalytic performance of $SrRuO_3$ using DFT theoretical calculations. Fig. 1a depicts the free energy diagram of $SrRuO_3$ and Sr_2RuIrO_6 in relation to the OER. At zero potential (U = 0 V), the Gibbs free energy changes (ΔG) for the rate-determining step (RDS, *OOH formation) were determined to be 2.47 and 2.23 eV for $SrRuO_3$ and Sr_2RuIrO_6, respectively. Upon the application of a potential (U = 1.23 V), these ΔG values decreased to 1.24 and 1.0 eV at the RDS for $SrRuO_3$ and Sr_2RuIrO_6, respectively. Furthermore, the density of states (DOS) for the Ru 4d and O 2p orbitals were investigated, as shown in Fig. 1b. The DOS of $SrRuO_3$ and Sr_2RuIrO_6 revealed that in Sr_2RuIrO_6, there is a reduction in the values to −2.19 and −3.21 eV in the Ru 4d and O 2p bands, respectively, compared to −1.53 and −2.15 eV in $SrRuO_3$. This indicates a downshift of the Ru 4d and O 2p orbitals in Sr_2RuIrO_6 relative to the Fermi level. The negative shift in the O 2p band center of Sr_2RuIrO_6 suggests an increased distance between the O 2p band center and the Fermi level, resulting in a reduced covalency of the Ru–O bond.[37,41] It is well-known that Ru-based catalysts are prone to instability due to the strong covalent bond between Ru and O, which leads to the participation of lattice oxygen in the reaction and the formation of soluble $Ru^{>4+}$ species.[23] Theoretical analysis suggests that the introduction of heteroatoms optimizes the band structure and the covalence of the metal–oxygen bond. To further minimize the reliance on precious metals, dual-site regulation was implemented for $SrRuO_3$. It was discovered that the best performance is achieved when the ratio of Ru to Ir is maintained at 2 : 1.

A series of $Sr_xCa_{3-x}Ru_2IrO_9$ perovskite oxides were synthesized using a simple sol–gel method. The X-ray diffraction (XRD) patterns in Fig. 2a and Fig. S1† indicate that the obtained catalysts possessed an orthorhombic phase with lattice parameters of a = 5.581 Å, b = 7.89 Å, c = 5.589 Å, and space group *ibmm* (number 74) at a 90 × 90 × 90 angle. Scanning electron microscopy (SEM) and transmission electron microscopy (TEM) images revealed $Sr_2CaRu_2IrO_9$ with slightly etched cubic nanomaterials ranging in size from 100 to 500 nm (Fig. 2b, d and Fig. S2†). Energy dispersive analysis (EDS) confirmed that Sr, Ca, Ru, Ir and O elements are uniformly distributed in the $Sr_2CaRu_2IrO_9$ sample, and the atomic ratio of Sr : Ca and Ru : Ir in the sample is about 2 : 1 (Fig. 2c and Fig. S3†).

The high-resolution transmission electron microscopy (HRTEM) images in Fig. 2e reveal distinct lattice fringes with a lattice spacing of 0.27 nm, corresponding to the (200) and (121) planes of $Sr_2CaRu_2IrO_9$. Compared to the standard unit cell of $SrRuO_3$, the lattice spacing of $Sr_3Ru_2IrO_9$ is smaller. This change is attributed to the contraction of the lattice caused by replacing Sr with Ca, which has a smaller ionic radius. Electron paramagnetic resonance (EPR) provides valuable information about the presence of unpaired electrons on the material's surface, serving as an indicator of oxygen vacancies. Specifically, the g factor value depends on the characteristics of the free radical present, with a g value around 2.00 indicating the presence of oxygen vacancies within the material.[42–44] In the EPR spectra of the obtained catalysts, a g value of approximately 2.003 was observed. Furthermore, introducing negative/cation species results in an increased intensity of a pair of symmetric peaks at g = 2.003, providing evidence for enhanced generation of oxygen vacancies in $Sr_2CaRu_2IrO_9$.

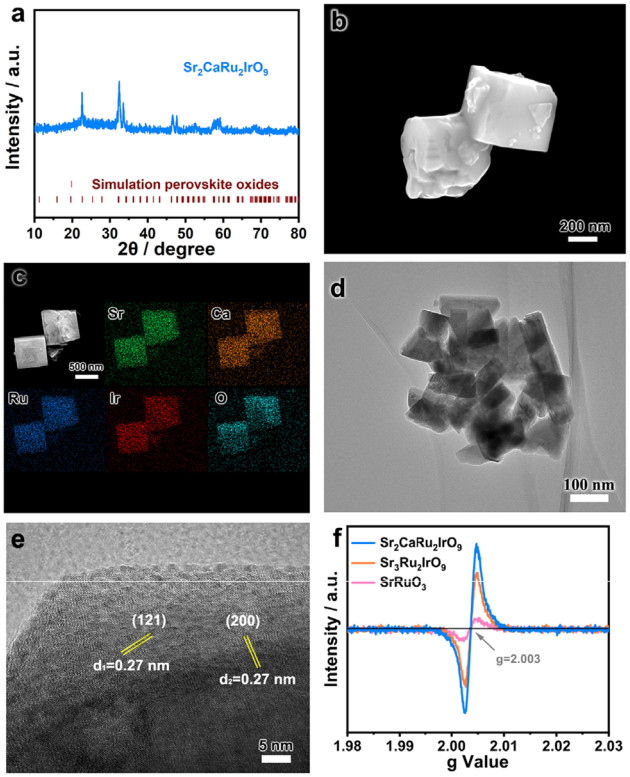

Fig. 2 (a) XRD, (b) SEM, (c) EDS mapping, (d) TEM and (e) HRTEM of $Sr_2CaRu_2IrO_9$, and (f) EPR spectra of $Sr_2CaRu_2IrO_9$, $Sr_3Ru_2IrO_9$ and $SrRuO_3$.

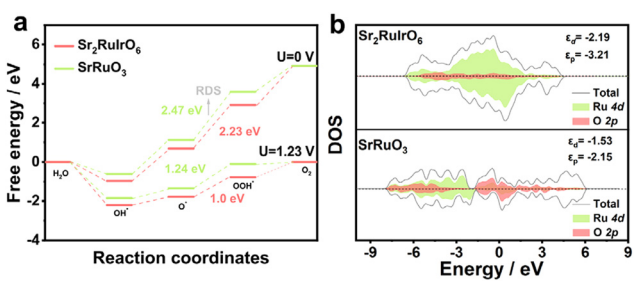

Fig. 1 (a) The free energy profiles of the OER process on $SrRuO_3$ and Sr_2RuIrO_6 under the applied overpotentials of 0 and 1.23 V (*vs.* RHE), respectively. (b) DOS of $SrRuO_3$ and Sr_2RuIrO_6.

The OER performances of $Sr_2CaRu_2IrO_9$ and other control samples were evaluated in a N_2-saturated 0.5 M H_2SO_4 electrolyte. Initially, the catalytic performance of $Sr_3Ru_xIr_{3-x}O_9$ ($x > 1.5$) perovskite oxide with a low Ir concentration was investigated. The results indicated that $Sr_3Ru_2IrO_9$ exhibited the best catalytic performance, when the Ru : Ir ratio was 2 : 1 (Fig. S4a†). Subsequently, A-site regulation was performed while maintaining the Ru : Ir ratio at 2 : 1, and the impact of A-site regulation on catalytic performance was explored. The LSV curves (Fig. S4b†) reveal that $Sr_2CaRu_2IrO_9$ shows the best catalytic performance, which is the focus of further research. Fig. 3a demonstrates that the catalytic activity of $Sr_2CaRu_2IrO_9$ (10 mA cm^{-2}, 172 mV) surpasses those of perovskite $SrRuO_3$ (10 mA cm^{-2}, 270 mV), $Sr_3Ru_2IrO_9$ (10 mA cm^{-2}, 185 mV), and commercial RuO_2 (10 mA cm^{-2}, 273 mV). Then, to further understand the reaction kinetics of the catalyst, the Tafel plot of the samples was analyzed. $Sr_2CaRu_2IrO_9$ (21.41 mV dec^{-1}) exhibits the lowest Tafel plot compared to other catalysts (Fig. 3b and Fig. S5†), such as commercial RuO_2 (61.07 mV dec^{-1}), $SrRuO_3$ (58.44 mV dec^{-1}), and $Sr_3Ru_2IrO_9$ (48.22 mV dec^{-1}). The smaller Tafel slope of $Sr_2CaRu_2IrO_9$ indicates a rapidly boosted current density with an increase in overpotential, which is typically a sign of a good catalyst.[46,47]

Stability is an essential criterion for evaluating catalytic performance. To assess the stability of the electrocatalysts in acidic media, chronopotentiometry was conducted in a 0.5 M H_2SO_4 solution. The results, as illustrated in Fig. 3c and Fig. S6,† demonstrate that the $Sr_2CaRu_2IrO_9$ electrocatalyst maintained its catalytic performance for 75 hours at a current density of 10 mA cm^{-2}, without any significant decline. This suggests that an appropriate amount of Ca doping can enhance the performance of the triple perovskite and improve its stability. To analyze the leaching of Sr, Ca, Ru, and Ir in $Sr_2CaRu_2IrO_9$, inductively coupled plasma atomic emission spectrometry (ICP-OES) was employed. In the stability test conducted for 8 hours (Fig. 3d), only a slight leaching of Sr, Ca, Ru, and Ir was observed. The TEM and HRTEM images taken after the OER (Fig. S7a and S7c†) revealed that the morphology and structure of the catalyst remained largely unchanged, with no formation of an amorphous layer on the surface. The XRD analysis after the OER also confirmed its excellent structural stability (Fig. S7b†). Based on these findings, it can be concluded that $Sr_2CaRu_2IrO_9$ demonstrates both high catalytic stability and good structural stability under acidic conditions. Additionally, it is important to note that the catalytic performance of $Sr_2CaRu_2IrO_9$ surpasses those of most reported acid oxygen evolution reaction catalysts (Fig. 3e).[23,26,31,35,45–51]

In order to further investigate the reasons behind its activity, several electrochemical tests were conducted. The results of the electrochemical impedance spectroscopy (EIS) tests showed that the $Sr_2CaRu_2IrO_9$ catalyst exhibited the smallest charge transfer resistance, indicating faster reaction kinetics (Fig. 4a and Fig. S8†). This enhanced reaction kinetics can be attributed to the presence of a greater number of oxygen vacancies (V_O) in $Sr_2CaRu_2IrO_9$. The increased oxygen vacancies promote the electrical conductivity of the catalyst, which is responsible for its improved catalytic performance. To evaluate the electrochemical specific surface area (ECSA) of the catalyst, a cyclic voltammetry (CV) test was performed to determine the double layer capacitance (C_{dl}, Fig. S9†), which is directly proportional to the ECSA. The C_{dl} value of the

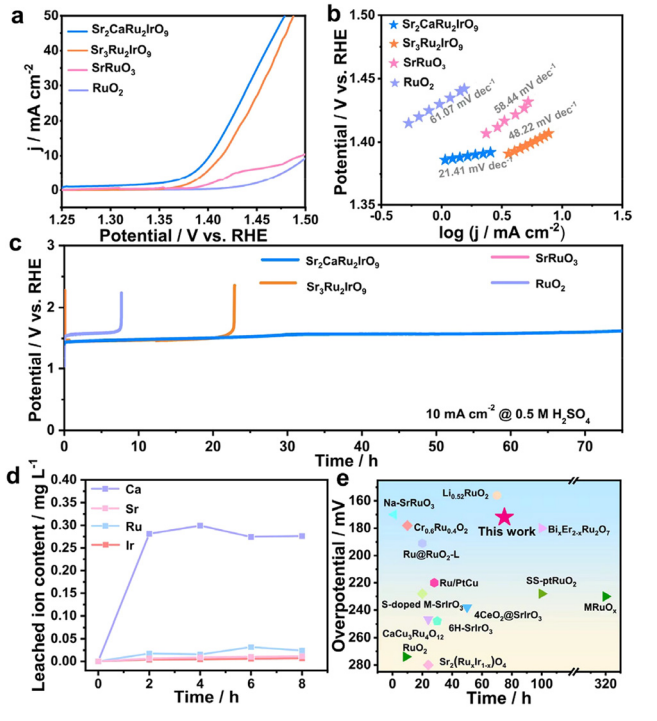

Fig. 3 (a) LSV curves, (b) Tafel slope and (c) chronopotentiometry curve toward the OER of $Sr_2CaRu_2IrO_9$, $Sr_3Ru_2IrO_9$, $SrRuO_3$ and commercial RuO_2, (d) contents of leached metals of $Sr_2CaRu_2IrO_9$, and (e) comparison of OER performance with representative acidic water oxidation electrocatalysts.

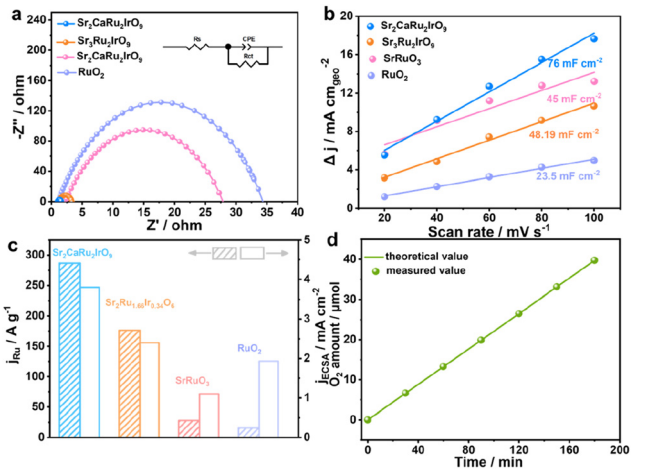

Fig. 4 (a) Nyquist curves, (b) double-layer capacitance, (c) mass activity and ECSA-normalized specific activities of $Sr_2CaRu_2IrO_9$, $Sr_3Ru_2IrO_9$, $SrRuO_3$, and commercial RuO_2, and (d) faradaic efficiency of $Sr_2CaRu_2IrO_9$.

$Sr_2CaRu_2IrO_9$ catalyst was found to be 76 mF cm^{-2} (Fig. 4b), which is higher than those of commercial RuO_2 and $SrRuO_3$, and slightly lower than those of Sr_2RuIrO_6 and $Sr_3Ru_2IrO_9$. The higher C_{dl} value of $Sr_2CaRu_2IrO_9$ indicates that it possesses more active sites for catalytic reactions. As shown in Fig. 4c, the catalytic activities of $Sr_2CaRu_2IrO_9$, $Sr_3Ru_2IrO_9$, $SrRuO_3$, and RuO_2 are normalized by electrochemical specific surface area and mass activity. The results show that $Sr_2CaRu_2IrO_9$ has higher intrinsic activity and better catalytic performance with less catalyst. Upon comparison of the turnover frequencies (TOF) at 1.47 V (Fig. S10†), it is observed that the TOF of $Sr_2CaRu_2IrO_9$ is 2.11 s^{-1}, which is significantly higher than those of $Sr_3Ru_2IrO_9$ (1.88 s^{-1}), $SrRuO_3$ (0.78 s^{-1}), and RuO_2 (0.53 s^{-1}). It is also evident that $Sr_2CaRu_2IrO_9$ exhibits the best intrinsic activity in this comparison. The faradaic efficiency, calculated from the actual oxygen production, is in good agreement with the trend of the theoretical value. This indicates that the as-prepared catalyst exhibits not only good activity but also high selectivity in the OER process (Fig. 4d).

XPS analysis was conducted to further investigate the correlation between the electronic structure and catalytic performance. The changes in the electronic structure of $Sr_2CaRu_2IrO_9$ before and after the OER were explored. As shown in Fig. 5a and b, the intensity of Sr 3d and Ca 2p significantly decreases in $Sr_2CaRu_2IrO_9$ after the OER. This can be attributed to the slight leaching of Sr and Ca during the catalytic process, which is consistent with the ICP-OES results. On the other hand, Fig. 5c and d illustrate that the Ru 3p and Ir 4f peaks of $Sr_2CaRu_2IrO_9$ remain almost unchanged before and after the OER. In the case of Ru-based catalysts, they are prone to exist in an unstable high-valence state during the acidic OER, leading to poor catalyst stability.[33,36,40] The XPS results demonstrate that the dual-site regulation prevents the formation of soluble $Ru^{>4+}$ species, thereby effectively enhancing the catalyst's corrosion resistance.

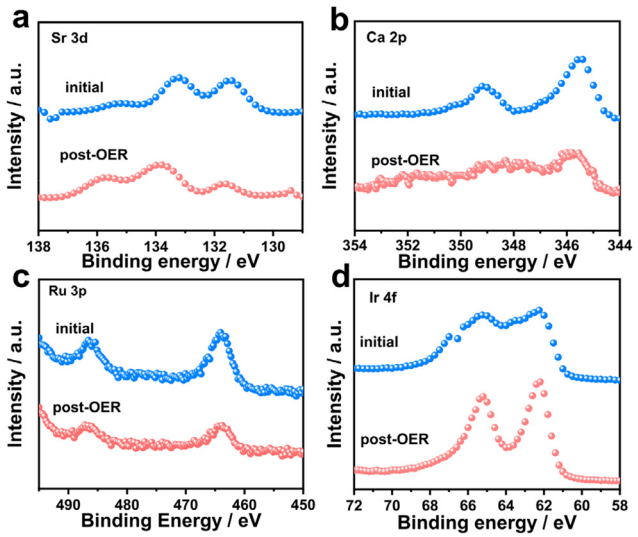

Fig. 5 High-resolution XPS spectra (a) Sr 3d, (b) Ca 2p, (c) Ru 3p and (d) Ir 4f of $Sr_2CaRu_2IrO_9$ before and after the OER.

A comparison of the O 1s high-resolution XPS spectrum between $Sr_2CaRu_2IrO_9$ and $Sr_3Ru_2IrO_9$ was conducted. As depicted in Fig. 6a and b, three peaks at 529.2, 530.75, and 532.8 eV were observed, corresponding to lattice oxygen (O_L), oxygen vacancies (V_O), and adsorbed oxygen (O_{ads}), respectively.[43,44] The results indicate that $Sr_2CaRu_2IrO_9$ has a higher concentration of oxygen vacancies than $Sr_3Ru_2IrO_9$, which is the primary reason for its superior OER activity. Furthermore, the changes in the O_L and V_O contents of $Sr_2CaRu_2IrO_9$ and $Sr_3Ru_2IrO_9$ before and after the OER were compared (Fig. 6c). The obtained $Sr_2CaRu_2IrO_9$ exhibited only slight changes in the content of O_L and V_O during the OER. In contrast, $Sr_3Ru_2IrO_9$ had a significant amount of O_L involved in the reaction process during the OER, leading to the formation of a large number of V_O. An appropriate amount of V_O effectively suppresses the interaction between the adsorbate intermediate and lattice oxygen, thus improving the stability of $Sr_2CaRu_2IrO_9$.[52–54] Additionally, the OER catalytic reaction mechanism was further analyzed through *in situ* Raman testing. Fig. 6d depicts the Raman spectra of the catalyst at 1.3–1.5 V. The Raman bands at 424 and 883 cm^{-1} correspond to E_g and B_{2g} of $Sr_2CaRu_2IrO_9$, while the peak at 489 cm^{-1} is characteristic of F_{2g} lattice oxygen, and the peak at 587 cm^{-1} corresponds to V_O.[55–58] Based on Raman analysis, it is evident that the catalyst itself contains a significant amount of oxygen vacancies, which effectively enhances the catalytic reaction. However, as the voltage increases, there is no significant change in the intensity of the oxygen vacancy Raman peak of the catalyst. This indicates that the presence of abundant oxygen vacancies in the catalyst hinders further involvement of lattice oxygen in the OER, thereby impeding the formation of additional oxygen vacancies. These findings suggest that $Sr_2CaRu_2IrO_9$ exhibits exceptional structural and catalytic stability, as supported by our Raman test results consistent with those of performance tests and XPS analysis.

In addition, the impact of dual-site substitution on the electronic structure and catalytic performance of the catalyst was

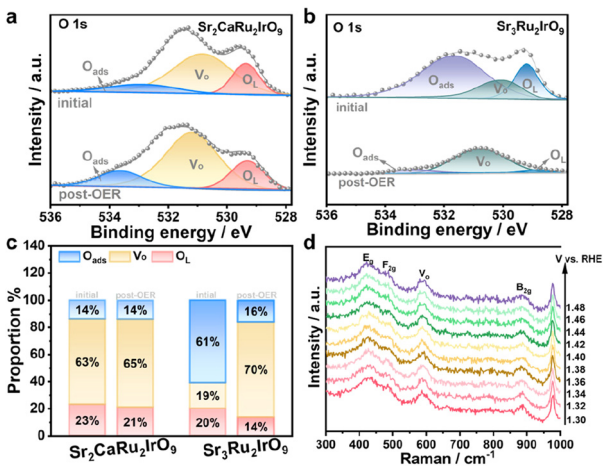

Fig. 6 (a and b) O 1s XPS spectra and (c) the proportion of O_{ads}, O_L and V_O of $Sr_2CaRu_2IrO_9$ and $Sr_3Ru_2IrO_9$, and (d) *in situ* Raman spectroscopy of the $Sr_2CaRu_2IrO_9$ for 0.5 M H_2SO_4 at varied potentials.

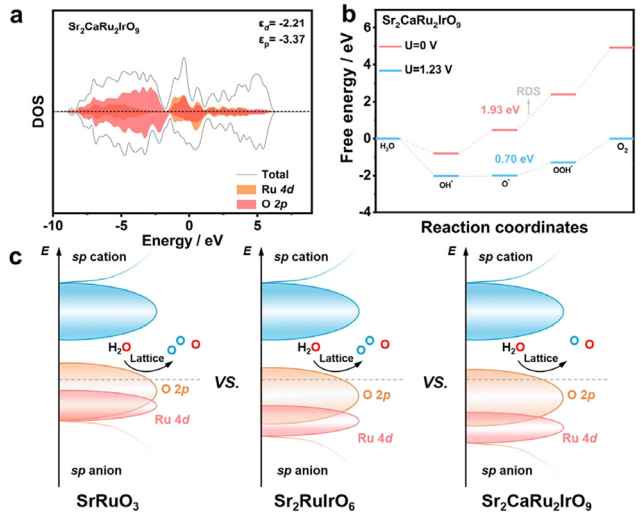

Fig. 7 (a) DOS, (b) the free energy profiles of the OER process under the applied overpotentials of 0 and 1.23 V (*vs.* RHE), and (c) schematic diagrams of rigid band models for $SrRuO_3$, Sr_2RuIrO_6 and $Sr_2CaRu_2IrO_9$ toward the acidic OER.

investigated through density functional theory (DFT) calculations.[55,58] The d-band center of the active metal plays a pivotal role in determining the strength of binding between the metal site and the adsorbed oxygen. The density of state curve (DOS, Fig. 7a and 1b) reveals that the Ru d-band center of $Sr_2CaRu_2IrO_9$, Sr_2RuIrO_6, and $SrRuO_3$ is located at −2.21, −2.19, and −1.53 eV, respectively. This indicates that the introduction of two sites shifts the d-band center of the $Sr_2CaRu_2IrO_9$ catalyst further away from the Fermi level. Consequently, this results in a weaker binding strength between Ru and O, optimizing the adsorption energy ($\Delta G_{HOO^*} - \Delta G_{O^*}$ = 1.93 eV) and enhancing the catalytic activity (Fig. 7b). In addition, the participation of lattice oxygen in the LOM, which leads to a significant generation of V_O, is the key factor contributing to the severe deactivation of OER catalysts. While an appropriate amount of V_O can enhance the conductivity of the catalyst, an excessive amount can result in lattice collapse. To address this issue, a viable strategy is to expand the O 2p centers, which effectively suppresses the excessive formation of V_O. Notably, $Sr_2CaRu_2IrO_9$ exhibits a significantly enlarged p-band center and shifts downward compared to Sr_2RuIrO_6 and $SrRuO_3$ (Fig. 7c). These findings indicate that the dual-site introduction weakens the covalency of Ru–O bonds, thereby inhibiting the excessive generation of V_O during catalytic processes. Ultimately, this approach slows down the over-oxidation of Ru species to soluble RuO_4 and improves catalytic stability.

Conclusions

In summary, a triple perovskite $Sr_2CaRu_2IrO_9$ has been successfully synthesized as an efficient electrocatalyst for the acidic oxygen evolution reaction. The $Sr_2CaRu_2IrO_9$ catalyst exhibited a remarkably low overpotential of only 172 mV to achieve a current density of 10 mA cm^{-2} in 0.5 M H_2SO_4 and maintained its catalytic performance for over 75 hours. The generation of oxygen vacancies effectively balances the participation of AEM and LOM in the OER and suppresses the formation of expensive soluble Ru species, thereby enhancing the activity and stability of the catalyst. Furthermore, the DFT calculations identify that the introduction of dual-site heteroatoms weakens the covalency of Ru–O and optimizes the adsorption energy of oxygen intermediates, improving the inherent catalytic activity and stability. This study presents a feasible strategy for developing stable and efficient acidic OER catalysts and demonstrates the potential of noble metal-based catalysts in proton-exchange membrane water electrolyzers.

Author contributions

C. Liu, Y. Wu and G. Che designed the experiments and wrote the manuscript. Y. Wu and T. Xia synthesized, characterized, and analyzed the materials and wrote the manuscript. L. Yang, F. Guo, W. Jiang, J. Lang, Y. Ma and J. Feng assisted T. Xia with the materials synthesis, electrochemical measurements and analysis. All of the authors have read the manuscript and agree with its content.

Data availability

Data are available from the authors on reasonable request.

Conflicts of interest

There are no conflicts to declare.

Acknowledgements

This work acknowledges the financial support from the National Natural Science Foundation of China (NSFC, grant no. 52073283, 22078124, and 22378158); Natural Science Foundation Project of Jilin Province (YDZJ202201ZYTS336); Key Projects of Science and Technology Development Plan of Jilin Province (20220201125GX); the Project of Education Department of Jilin Province (JJKH20221155KJ); the Project of Jilin Province Development and Reform Commission (2023C032-2 and 2023C032-5); the Program for the Development of Science and Technology of Jilin Province (20230508040RC), and the Science and Technology Innovation Center Project of Jilin Province (YDZJ202102CXJD049).

References

1 J. Jin, J. Yin, Y. Hu, Y. Zheng, H. Liu, X. Wang, P. Xi and C. Yan, Stabilizing Sulfur Sites in Tetraoxygen Tetrahedral

Coordination Structure for Efficient Electrochemical Water Oxidation, *Angew. Chem.*, 2024, **136**, e202313185.
2 K. E. Trenberth, L. Cheng, P. Jacobs, Y. Zhang and J. Fasullo, Hurricane Harvey Links to Ocean Heat Content and Climate Change Adaptation, *Earths Future*, 2018, **6**, 730–744.
3 J. Jin, X. Wang, Y. Hu, Z. Zhang, H. Liu, J. Yin and P. Xi, Precisely Control Relationship between Sulfur Vacancy and H Absorption for Boosting Hydrogen Evolution Reaction, *Nano-Micro Lett.*, 2024, **16**, 63.
4 D. Chen, T. Liu, P. Wang, J. Zhao, C. Zhang, R. Cheng, W. Li, P. Ji, Z. Pu and S. Mu, Ionothermal Route to Phase-Pure RuB_2 Catalysts for Efficient Oxygen Evolution and Water Splitting in Acidic Media, *ACS Energy Lett.*, 2020, **5**, 2909–2915.
5 P. A. DeSario, C. N. Chervin, E. S. Nelson, M. B. Sassin and D. R. Rolison, Competitive Oxygen Evolution in Acid Electrolyte Catalyzed at Technologically Relevant Electrodes Painted with Nanoscale RuO_2, *ACS Appl. Mater. Interfaces*, 2017, **9**, 2387–2395.
6 A. H. Abdol Rahim, A. S. Tijani, S. K. Kamarudin and S. Hanapi, An Overview of Polymer Electrolyte Membrane Electrolyzer for Hydrogen Production: Modeling and Mass Transport, *J. Power Sources*, 2016, **309**, 56–65.
7 S. Geiger, O. Kasian, M. Ledendecker, E. Pizzutilo, A. M. Mingers, W. Fu, O. Diaz-Morales, Z. Li, T. Oellers, L. Fruchter, A. Ludwig, K. J. J. Mayrhofer, M. T. M. Koper and S. Cherevko, The Stability Number as a Metric for Electrocatalyst Stability Benchmarking, *Nat. Catal.*, 2018, **1**, 508–515.
8 S. D. Ghadge, O. I. Velikokhatnyi, M. K. Datta, P. M. Shanthi, S. Tan, K. Damodaran and P. N. Kumta, Experimental and Theoretical Validation of High Efficiency and Robust Electrocatalytic Response of One-Dimensional (1D) (Mn, Ir)O_2:10F Nanorods for the Oxygen Evolution Reaction in PEM-Based Water Electrolysis, *ACS Catal.*, 2019, **9**, 2134–2157.
9 H. Jin, X. Liu, P. An, C. Tang, H. Yu, Q. Zhang, H. Peng, L. Gu, Y. Zheng, T. Song, K. Davey, U. Paik, J. Dong and S. Qiao, Dynamic Rhenium Dopant Boosts Ruthenium Oxide for Durable Oxygen Evolution, *Nat. Commun.*, 2023, **14**, 354.
10 W. Shen, Y. Zheng, Y. Hu, J. Jin, Y. Hou, N. Zhang, L. An, P. Xi and C. Yan, Rare-Earth-Modified NiS_2 Improves OH Coverage for an Industrial Alkaline Water Electrolyzer, *J. Am. Chem. Soc.*, 2024, **146**, 5324–5332.
11 P. Da, Y. Zheng, Y. Hu, Z. Wu, H. Zhao, Y. Wei, L. Guo, J. Wang, Y. Wei, S. Xi, C. Yan and P. Xi, Synthesis of Bandgap Tunable Transition Metal Sulfides through Gas Phase Cation Exchange Induced Topological Transformation, *Angew. Chem., Int. Ed.*, 2023, **62**, e202301802.
12 J. Li, Oxygen Evolution Reaction in Energy Conversion and Storage: Design Strategies Under and Beyond the Energy Scaling Relationship, *Nano-Micro Lett.*, 2022, **14**, 112.
13 L. Li, P. Wang, Q. Shao and X. Huang, Recent Progress in Advanced Electrocatalyst Design for Acidic Oxygen Evolution Reaction, *Adv. Mater.*, 2021, **33**, 2004243.
14 J. Liang, F. Ma, S. Hwang, X. Wang, J. Sokolowski, Q. Li, G. Wu and D. Su, Atomic Arrangement Engineering of Metallic Nanocrystals for Energy-Conversion Electrocatalysis, *Joule*, 2019, **3**, 956–991.
15 Y. Lin, Y. Dong, X. Wang and L. Chen, Electrocatalysts for Oxygen Evolution Reaction in Acidic Media, *Adv. Mater.*, 2023, **35**, 2210565.
16 Y. Lin, Z. Tian, L. Zhang, J. Ma, Z. Jiang, B. J. Deibert, R. Ge and L. Chen, Chromium-Ruthenium Oxide Solid Solution Electrocatalyst for Highly Efficient Oxygen Evolution Reaction in Acidic Media, *Nat. Commun.*, 2019, **10**, 162.
17 I. C. Man, H. Su, F. Calle-Vallejo, H. A. Hansen, J. I. Martínez, N. G. Inoglu, J. Kitchin, T. F. Jaramillo, J. K. Nørskov and J. Rossmeisl, Universality in Oxygen Evolution Electrocatalysis on Oxide Surfaces, *ChemCatChem*, 2011, **3**, 1159–1165.
18 P. Millet, R. Ngameni, S. A. Grigoriev, N. Mbemba, F. Brisset, A. Ranjbari and C. Etiévant, PEM Water Electrolyzers: From Electrocatalysis to Stack Development, *Int. J. Hydrogen Energy*, 2010, **35**, 5043–5052.
19 Z. Shi, J. Li, Y. Wang, S. Liu, J. Zhu, J. Yang, X. Wang, J. Ni, Z. Jiang, L. Zhang, Y. Wang, C. Liu, W. Xing and J. Ge, Customized Reaction Route for Ruthenium Oxide Towards Stabilized Water Oxidation in High-Performance PEM Electrolyzers, *Nat. Commun.*, 2023, **14**, 843.
20 H. J. Song, H. Yoon, B. Ju and D. W. Kim, Highly Efficient Perovskite-Based Electrocatalysts for Water Oxidation in Acidic Environments: A Mini Review, *Adv. Energy Mater.*, 2020, **11**, 2002428.
21 M. You, L. Gui, X. Ma, Z. Wang, Y. Xu, J. Zhang, J. Sun, B. He and L. Zhao, Electronic Tuning of $SrIrO_3$ Perovskite Nanosheets by Sulfur Incorporation to Induce Highly Efficient and Long-Lasting Oxygen Evolution in Acidic Media, *Appl. Catal., B*, 2021, **298**, 120562.
22 Y. Sun, R. Li, X. Chen, J. Wu, Y. Xie, X. Wang, K. Ma, L. Wang, Z. Zhang, Q. Liao, Z. Kang and Y. Zhang, A-Site, Management Prompts the Dynamic Reconstructed Active Phase of Perovskite Oxide OER Catalysts, *Adv. Energy Mater.*, 2021, **11**, 2003755.
23 X. Miao, L. Zhang, L. Wu, Z. Hu, L. Shi and S. Zhou, Quadruple Perovskite Ruthenate as a Highly Efficient Catalyst for Acidic Water Oxidation, *Nat. Commun.*, 2019, **10**, 3809.
24 L. Yang, G. Yu, X. Ai, W. Yan, H. Duan, W. Chen, X. Li, T. Wang, C. Zhang, X. Huang, J. Chen and X. Zou, Efficient Oxygen Evolution Electrocatalysis in Acid by a Perovskite with Face-Sharing IrO_6 Octahedral Dimers, *Nat. Commun.*, 2018, **9**, 5236.
25 H. Liu, Z. Zhang, M. Li, Z. Wang, X. Zhang, T. Li, Y. Li, S. Tian, Y. Kuang and X. Sun, Iridium Doped Pyrochlore Ruthenates for Efficient and Durable Electrocatalytic Oxygen Evolution in Acidic Media, *Small*, 2022, **18**, 2202513.

26 S. Wang, S. Yang, Z. Wei, Y. Liang, J. Zhu, Y. Tang and X. Qiu, Ultrathin IrRu Nanocages with Tunable Electronic Reciprocity for Highly Efficient Water Splitting in Acidic Media, *J. Mater. Chem. A*, 2022, **10**, 25556.

27 L. Yang, L. Shi, H. Chen, X. Liang, B. Tian, K. Zhang, Y. Zou and X. Zou, A Highly Active, Long-Lived Oxygen Evolution Electrocatalyst Derived from Open-Framework Iridates, *Adv. Mater.*, 2023, **35**, 2208539.

28 M. Povia, D. F. Abbott, J. Herranz, A. Heinritz, D. Lebedev, B. J. Kim, E. Fabbri, A. Patru, J. Kohlbrecher, R. Schäublin, M. Nachtegaal, C. Copéret and T. J. Schmidt, Operando X-Ray Characterization of High Surface Area Iridium Oxides to Decouple Their Activity Losses for the Oxygen Evolution Reaction, *Energy Environ. Sci.*, 2019, **12**, 3038–3052.

29 Y. Wang, R. Yang, Y. Ding, B. Zhang, H. Li, B. Bai, M. Li, Y. Cui, J. Xiao and Z. Wu, Unraveling Oxygen Vacancy Site Mechanism of Rh-Doped RuO_2 Catalyst for Long-Lasting Acidic Water Oxidation, *Nat. Commun.*, 2023, **14**, 1412.

30 L. An, C. Wei, M. Lu, H. Liu, Y. Chen, G. G. Scherer, A. C. Fisher, P. Xi, Z. J. Xu and C. Yan, Recent Development of Oxygen Evolution Electrocatalysts in Acidic Environment, *Adv. Mater.*, 2021, **33**, 2006328.

31 Q. Wang, Y. Cheng, H. Tao, Y. Liu, X. Ma, D. Li, H. Yang and B. Liu, Long-Term Stability Challenges and Opportunities in Acidic Oxygen Evolution Electrocatalysis, *Angew. Chem., Int. Ed.*, 2023, **62**, e202216645.

32 Z. Chen, L. Guo, L. Pan, T. Yan, Z. He, Y. Li, C. Shi, Z. Huang, X. Zhang and J. Zou, Advances in Oxygen Evolution Electrocatalysts for Proton Exchange Membrane Water Electrolyzers, *Adv. Energy Mater.*, 2022, **12**, 2103670.

33 J. Wang, C. Cheng, Q. Yuan, H. Yang, F. Meng, Q. Zhang, L. Gu, J. Cao, L. Li, S. Haw, Q. Shao, L. Zhang, T. Cheng, F. Jiao and X. Huang, Exceptionally Active and Stable RuO_2 with Interstitial Carbon for Water Oxidation in Acid, *Chem*, 2022, **8**, 1673–1687.

34 H. Chen, M. Zhang, Y. Wang, K. Sun, L. Wang, Z. Xie, Y. Shen, X. Han, L. Yang and X. Zou, Crystal Phase Engineering of Electrocatalysts for Energy Conversions, *Nano Res.*, 2022, **15**, 10194–10217.

35 F. Wang, C. Zhang and H. Yang, Mixed B-Site Ruddlesden-Popper Phase $Sr_2(Ru_xIr_{1-x})O_4$ Enables Enhanced Activity for Oxygen Evolution Reaction, *J. Energy Chem.*, 2022, **70**, 623–629.

36 I. Rodríguez-García, D. Galyamin, L. Pascual, P. Ferrer, M. A. Peña, D. Grinter, G. Held, M. A. Salam, M. Mokhtar, K. Narasimharao, M. Retuerto and S. Rojas, Enhanced Stability of $SrRuO_3$ Mixed Oxide Via Monovalent Doping in $Sr_{1-x}K_xRuO_3$ for the Oxygen Evolution Reaction, *J. Power Sources*, 2022, **521**, 230950.

37 S. Hao, M. Liu, J. Pan, X. Liu, X. Tan, N. Xu, Y. He, L. Lei and X. Zhang, Dopants Fixation of Ruthenium for Boosting Acidic Oxygen Evolution Stability and Activity, *Nat. Commun.*, 2020, **11**, 5368.

38 Z. Y. Wu, F. Y. Chen, B. Li, S. W. Yu, Y. Z. Finfrock, D. M. Meira, Q. Q. Yan, P. Zhu, M. X. Chen, T. W. Song, Z. Yin, H. W. Liang, S. Zhang, G. Wang and H. Wang, Non-Iridium-Based Electrocatalyst for Durable Acidic Oxygen Evolution Reaction in Proton Exchange Membrane Water Electrolysis, *Nat. Mater.*, 2023, **22**, 100–108.

39 N. Yao, H. Jia, J. Zhu, Z. Shi, H. Cong, J. Ge and W. Luo, Atomically Dispersed Ru Oxide Catalyst with Lattice Oxygen Participation for Efficient Acidic Water Oxidation, *Chem*, 2023, **9**, 1882–1896.

40 Y. Xue, J. Zhao, L. Huang, Y. R. Lu, A. Malek, G. Gao, Z. Zhuang, D. Wang, C. T. Yavuz and X. Lu, Stabilizing Ruthenium Dioxide with Cation-anchored Sulfate for Durable Oxygen Evolution in Proton-Exchange Membrane Water Electrolyzers, *Nat. Commun.*, 2023, **14**, 8093.

41 Y. Xu, Z. Mao, J. Zhang, J. Ji, Y. Zou, M. Dong, B. Fu, M. Hu, K. Zhang, Z. Chen, S. Chen, H. Yin, P. Liu and H. Zhao, Strain-modulated Ru-O Covalency in Ru-Sn Oxide Enabling Efficient and Stable Water Oxidation in Acidic Solution, *Angew. Chem.*, 2024, **136**, e202316029.

42 J. Ye, P. Li, H. Zhang, *et al.*, Manipulating Oxygen Vacancies to Spur Ion Kinetics in V_2O_5 Structures for Superior Aqueous Zinc-Ion Batteries, *Adv. Funct. Mater.*, 2023, **33**, 2305659.

43 Y. H. Wang, L. Li, J. Shi, M. Y. Xie, J. Nie, G. F. Huang, B. Li, W. Hu, A. Pan and W. Q. Huang, Oxygen Defect Engineering Promotes Synergy Between Adsorbate Evolution and Single Lattice Oxygen Mechanisms of OER in Transition Metal-Based (oxy) Hydroxide, *Adv. Sci.*, 2023, **10**, 2303321.

44 Z. F. Huang, J. Song, Y. Du, S. B. Xi, S. Dou, J. M. V. Nsanzimana, C. Wang, Z. C. J. Xu and X. Wang, Chemical and Structural Origin of Lattice Oxygen Oxidation in Co-Zn Oxyhydroxide Oxygen Evolution Electrocatalysts, *Nat. Energy*, 2019, **4**, 329–338.

45 Y. Wen, T. Yang, C. Cheng, X. Zhao, E. Liu and J. Yang, Engineering Ru(IV) Charge Density in $Ru@RuO_2$ Core-Shell Electrocatalyst Via Tensile Strain for Efficient Oxygen Evolution in Acidic Media, *Chin. J. Catal.*, 2020, **41**, 1161–1167.

46 M. Retuerto, L. Pascual, F. Calle-Vallejo, P. Ferrer, D. Gianolio, A. G. Pereira, A. García, J. Torrero, M. T. Fernandez-Díaz, P. Bencok, M. A. Pena, J. L. G. Fierro and S. Rojas, Na-Doped Ruthenium Perovskite Electrocatalysts with Improved Oxygen Evolution Activity and Durability in Acidic Media, *Nat. Commun.*, 2019, **10**, 2041.

47 Y. Lin, Z. Tian, L. Zhang, J. Ma, Z. Jiang, B. J. Deibert, R. Ge and L. Chen, Chromium-Ruthenium Oxide Solid Solution Electrocatalyst for Highly Efficient Oxygen Evolution Reaction in Acidic Media, *Nat. Commun.*, 2019, **10**, 162.

48 G. Zhou, P. Wang, B. Hu, X. Shen, C. Liu, W. Tao, P. Huang and L. Liu, Spin-Related Symmetry Breaking Induced by Half-Disordered Hybridization in $BixEr_{2-x}Ru_2O_7$ Pyrochlores for Acidic Oxygen Evolution, *Nat. Commun.*, 2022, **13**, 4106.

49 J. Wang, H. Yang, F. Li, L. Li, J. Wu, S. Liu, T. Cheng, Y. Xu, Q. Shao and X. Huang, Single-Site Pt-Doped RuO_2 Hollow

Nanospheres with Interstitial C for High-Performance Acidic Overall Water Splitting, *Sci. Adv.*, 2022, **8**, e9271.

50 M. You, Y. Xu, B. He, J. Zhang, L. Gui, J. Xu, W. Zhou and L. Zhao, Realizing Robust and Efficient Acidic Oxygen Evolution by Electronic Modulation of 0D/2D CeO_2 Quantum Dots Decorated $SrIrO_3$ Nanosheets, *Appl. Catal., B*, 2022, **315**, 121579.

51 Y. Yao, S. Hu, W. Chen, Z. Huang, W. Wei, T. Yao, R. Liu, K. Zang, X. Wang, G. Wu, W. Yuan, T. Yuan, B. Zhu, W. Liu, Z. Li, D. He, Z. Xue, Y. Wang, X. Zheng, J. Dong, C. Chang, Y. Chen, X. Hong, J. Luo, S. Wei, W. Li, P. Strasser, Y. Wu and Y. Li, Engineering the Electronic Structure of Single Atom Ru Sites Via Compressive Strain Boosts Acidic Water Oxidation Electrocatalysis, *Nat. Catal.*, 2019, **2**, 304–313.

52 P. Sun, Z. Qiao, X. Dong, R. Jiang, Z. Hu, J. Yun and D. Cao, Designing 3d Transition Metal Cation-Doped $MRuO_x$ as Durable Acidic Oxygen Evolution Electrocatalysts for PEM Water Electrolyzers, *J. Am. Chem. Soc.*, 2024, **146**, 15515–15524.

53 Y. Wen, P. Chen, L. Wang, S. Li, Z. Wang, J. Abed, X. Mao, Y. Min, C. T. Dinh, P. D. Luna, R. Huang, L. Zhang, L. Wang, L. Wang, R. J. Nielsen, H. Li, T. Zhuang, C. Ke, O. Voznyy, Y. Hu, Y. Li, W. A. Goddard III, B. Zhang, H. Peng and E. H. Sargent, Stabilizing Highly Active Ru Sites by Suppressing Lattice Oxygen Participation in Acidic Water Oxidation, *J. Am. Chem. Soc.*, 2021, **143**, 6482–6490.

54 S. Zhao, S. F. Hung, L. Deng, W. J. Zeng, T. Xiao, S. Li, C. H. Kuo, H. Y. Chen, F. Hu and S. Peng, Constructing Regulable Supports *via* Non-Stoichiometric Engineering to Stabilize Ruthenium Nanoparticles for Enhanced pH-Universal Water Splitting, *Nat. Commun.*, 2024, **15**, 2728.

55 J. Jin, J. Yin, H. Liu, B. Huang, Y. Hu, H. Zhang, M. Sun, Y. Peng, P. Xi and C. Yan, Atomic Sulfur Filling Oxygen Vacancies Optimizes H Absorption and Boosts the Hydrogen Evolution Reaction in Alkaline Media, *Angew. Chem.*, 2021, **133**, 14236–14242.

56 N. I. Kim, Y. J. Sa, T. S. Yoo, S. R. Choi, R. A. Afzal, T. Choi, Y. S. Seo, K. S. Lee, J. Y. Hwang and W. S. Choi, Oxygen-Deficient Triple Perovskites as Highly Active and Durable Bifunctional Electrocatalysts for Oxygen Electrode Reactions, *Sci. Adv.*, 2018, **4**, e9360.

57 A. K. Tomar, U. N. Pan, N. H. Kim and J. H. Lee, Enabling Lattice Oxygen Participation in a Triple Perovskite Oxide Electrocatalyst for the Oxygen Evolution Reaction, *ACS Energy Lett.*, 2022, **8**, 565–573.

58 M. Lu, Y. Zheng, Y. Hu, B. Huangs, D. Ji, M. Sun, J. Li, Y. Peng, R. Si, P. Xi and C. Yan, Artificially Steering Electrocatalytic Oxygen Evolution Reaction Mechanism by Regulating Oxygen Defect Contents in Perovskites, *Sci. Adv.*, 2022, **8**, e3563.